Self-Assembly of Active Bi_2O_3/TiO_2 Visible Photocatalyst with Ordered Mesoporous Structure and Highly Crystallized Anatase

Zhenfeng Bian,[†] Jian Zhu,[†] Shaohua Wang,[†] Yong Cao,[‡] Xufang Qian,[†] and Hexing Li*,[†]

Department of Chemistry, Shanghai Normal University, Shanghai 200234, People's Republic of China, and Department of Chemistry, Fudan University, Shanghai 200433, People's Republic of China

Received: January 14, 2008; In Final Form: February 19, 2008

Bi_2O_3/TiO_2 nanocrystallines with ordered mesoporous structure are synthesized by ab evaporation-induced self-assembly method. During liquid-phase photocatalytic degradation of *p*-chlorophenol under visible illumination ($\lambda > 420$ nm), this catalyst exhibits high activity owing to the synergetic effects of both the Bi_2O_3-photosensitization and the unique structural characteristics. The Bi_2O_3-photosensitization of TiO_2 could extend the spectral response from UV to visible area, making the Bi_2O_3/TiO_2 photocatalyst easily activated by visible lights. The ordered mesoporous channels facilitate the diffusion of reactant molecules. Meanwhile, the high surface area could enhance the Bi_2O_3 dispersion, the light harvesting, and the reactant adsorption. Furthermore, the highly crystallized anatase may promote the transfer of photoelectrons from bulk to surface and thus inhibit their recombination with photoholes, leading to enhanced quantum efficiency.

Introduction

Photocatalysis is an active area of research in the field of heterogeneous catalysis owing to its potential applications in environmental cleaning and H-energy production. In most cases, photocatalytic degradation is conducted over the TiO_2 owing to its peculiarities of chemical inertness, no-photocorrosion, low cost, and nontoxicity.[1] However, practical applications of the TiO_2 are still quite limited, mainly due to the low quantum efficiency and the requirement of UV-illuminated activation. Photosentisizing TiO_2 has been proved a promising way to extend spectral response from UV area to visible region.[2−5] Most studies are focused on the organic photosensitizers while studies on the inorganic photosensitizers have been seldom reported. In the viewpoint of stability, photosensitization of TiO_2 with inorganic substrates is superior over that with organic substrates since the organic compounds usually suffer from degradation during photocatalysis. Bi_2O_3 is an important photosentisizer with a direct band gap of 2.8 eV.[6] As a result, the Bi_2O_3/TiO_2 could be easily activated by visible lights owing to the photosensitization by Bi_2O_3.[6,7] Design of TiO_2 with well-defined mesoporous structure is a promising way to achieve high photocatalytic activity since the ordered mesopore channels facilitate fast intraparticle molecular transfer.[8−10] While the large surface area may enhance the light harvesting, the adsorption for reactant molecules, and even the dispersion of Bi_2O_3 nanoparticles. Meanwhile, a high crystallization degree of photocatalysts is favorable for rapid transfer of photocharges from bulk to surface, which could inhibit the recombination between photoelectrons and holes, leading to enhanced quantum efficiency.[11,12] However, preparation of semiconductor oxides with both the ordered mesoporous structure and highly crystalline pore wall is usually a challenging task.[13−15] Although mesoporous TiO_2 has already been synthesized by Antonelli and co-workers in 1995,[16] only a few papers concerning the ordered mesoporous TiO_2 with crystalline walls have been found in the literature.[8−10,13−15,17] While the mesoporous crystallized Bi_2O_3/TiO_2 has never been reported so far. In the present paper, we report a new approach to prepare mesoporous Bi_2O_3/TiO_2 nanocrystalline-based evaporation induced self-assembly (EISA) method. During photodegradation of *p*-chlorophenol under visible light irradiation, this catalyst is much more active than Degussa P-25 and the Bi_2O_3/TiO_2 prepared by traditional sol−gel method. The promoting effects on the activity from the photosensitization, the ordered mesoporous channels, the high surface area, and the high crystallization degree are examined and discussed.

Experimental Section

Catalyst Preparation. The Bi_2O_3/TiO_2 samples were synthesized by the EISA method using $EO_{20}PO_{70}EO_{20}$ (P123, Aldrich) surfactant as a template. In a typical synthesis, 1.7 g of $TiCl_4$, 3.0 g of tetrabutyl titanate ($Ti(OBu)_4$), and a certain amount of $Bi(NO_3)_3{\cdot}5H_2O$ were added into 12.0 mL of ethanol solution containing 1.0 g of P123. A transparent sol was obtained after being stirred for 1.5 h at 0 °C, which was transferred into a Petri dish to form a uniform thin layer. After being aged at 40 and 100 °C for 24 h, respectively, the precursor was calcined at 350 °C for 4 h (0.5 °C/min) to remove surfactant template and other organic species. The as-prepared samples were denoted as *x*% Bi_2O_3/TiO_2, where *x*% refers to the Bi/Ti molar ratio. For comparison, the Bi_2O_3/TiO_2 samples were also prepared in the traditional sol−gel method without adding P123, which were designated as *x*% Bi_2O_3/TiO_2(SG).

Catalyst Characterization. The crystallographic properties were investigated by X-ray diffraction (XRD, Rigaku D/MAX-2000, Cu $K\alpha_1$), and the particle size was estimated using the Scherrer equation. The morphologies were observed by a transmission electron microscopy (TEM, JEOL JEM2010). Nitrogen adsorption−desorption isotherms were collected at 77 K by using Quantachrome NOVA 4000e Surface Area & Pore Size Analyzer. Based on the adsorption branches of N_2 adsorption−desorption isotherms, the surface area (S_{BET}), pore volume (V_P), and pore diameter (D_P) were calculated by using

* To whom correspondence should be addressed. E-mail: HexingLi@shnu.edu.cn. Fax: +86 21 64322272.
† Shanghai Normal University.
‡ Fudan University.

10.1021/jp800324t CCC: $40.75
Published on Web 03/28/2008

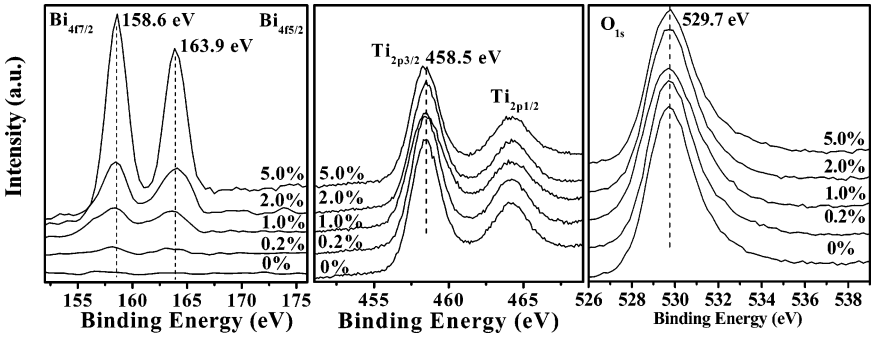

Figure 1. XPS spectra of samples with different Bi/Ti molar ratio.

BET and BJH models, respectively. Light absorbance was measured by UV−visible diffuse reflectance spectroscopy (DRS, MC-2530). Surface electronic states were analyzed by X-ray photoelectron spectroscopy (XPS, Perkin-Elmer PHI 5000C, Al Kα). All binding energies were calibrated by using the contaminant carbon (C_{1S} = 284.6 eV) as a reference. The Bi/Ti molar ratios were determined by means of inductively coupled plasma-atomic emission spectroscopy (ICP-AES, Jarrell-Ash Scan 2000).

Activity Test. The photocatalytic degradation of *p*-chlorophenol was carried out at 30 °C in an 80 mL self-designed quartz photochemical reactor containing 0.050 g of catalyst and 50 mL of 1.0×10^{-4} M *p*-chlorophenol aqueous solution. After reaching adsorption equilibrium, the photocatalytic reaction was initiated by irradiating the system with three 150 W xenon lamps located at 30 cm from the reaction solution. All the UV lights with wavelength shorter than 420 nm are removed by a glass filter (JB-420). After reaction for 6 h, the unreacted *p*-chlorophenol was analyzed by a UV spectrophotometer (UV 7504/PC) at its characteristic wavelength (λ = 224 nm), from which the degradation yield was calculated.[18] Preliminary tests demonstrated a good linear relationship between the light absorbance and the *p*-chlorophenol concentration. Only less than 3.0% *p*-chlorophenol decomposed after reaction for 6 h in the absence of either the photocatalyst or the light irradiation and, thus, could be neglected in comparison with the *p*-chlorophenol degraded via photocatalysis. The reproducibility of the photocatalytic degradation was checked by repeating the results at least three times and was found to be within acceptable limits (±5%).

Results and Discussion

Structural Characteristics. As shown in Figure 1, the XPS spectra demonstrated that all the Bi species in the as-prepared samples were present in the form of Bi_2O_3, corresponding to thebinding energies (BE) of 158.6 and 163.9 eV in $Bi_{4f7/2}$ and $Bi_{4f5/2}$ levels, respectively.[19] Such BE values were exactly the same as those obtained from pure Bi_2O_3. Meanwhile, the presence of Bi_2O_3 exerted no significant influence on the XPS spectra in either the Ti_{2P} level or the O_{1s} level. These results demonstrated that the Bi_2O_3 was present mainly as a separate phase in the Bi_2O_3/TiO_2 sample, i.e., the Bi species were not incorporated into the TiO_2 lattice. This could be attributed to the bigger size of Bi atom (103 pm) than that of the Ti atom (61 pm), which inhibited the replacement of Ti by Bi in the TiO_2 crystal lattice.[20]

Figure 2 shows the XRD patterns of the 1.0% Bi_2O_3/TiO_2 sample calcined at different temperatures. The low-angle XRD patterns (left) demonstrated that the Bi_2O_3/TiO_2 sample calcined at 300−350 °C displayed well-resolved peaks indicative of (100), (110), and (200) diffractions, suggesting a highly ordered

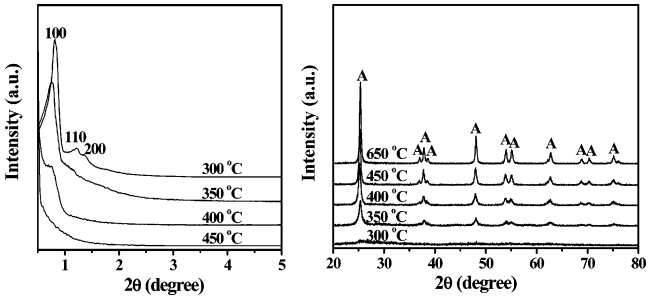

Figure 2. Low-angle XRD (left) and wide-angle XRD (right) patterns of 1.0% Bi_2O_3/TiO_2 calcined at elevated temperatures.

two-dimensional hexagonal mesoporous structure.[21] Increasing calcination temperature resulted in a gradual decrease of diffractional strength, showing a decrease in ordering degree of mesoporous structure. The principal diffractional peak (100) was still clearly observed even after being calcined at 400 °C, showing a relatively good thermal stability of the mesoporous structure. Further increase of the calcination temperature to 450 °C caused a complete collapse of the mesoporous structure, corresponding to the total disappearance of diffractional peaks. The wide-angle XRD patterns (right) revealed that the Bi_2O_3/TiO_2 sample calcined at 300 °C was present in amorphous state. After being calcined at 350 °C, the Bi_2O_3/TiO_2 sample displayed crystallized anatase phase corresponding to the characteristic diffractional peaks around 2θ of 25.2, 37.9, 47.8, 53.8, 55.0, 62.1, 62.7, 68.8, 70.3, and 75.1°, respectively. The crystallization degree could be enhanced slightly with the further increase of calcination temperature. No significant signals indicative of rutile appeared even after being calcined at 650 °C, indicating an excellent thermal stability against phase transformation. Based on the above results, we chose 350 °C as the optimum calcination temperature since the Bi_2O_3/TiO_2 calcined at that temperature displayed both the ordered mesoporous structure and highly crystallized anatase. No significant diffractional peaks indicative of Bi_2O_3 phase were observed in the Bi_2O_3/TiO_2 sample regardless of the calcination temperature, obviously owing to the extremely high dispersion.

As shown in Figure 3, all the Bi_2O_3/TiO_2 samples with Bi/Ti molar ratio ranging from 0 to 5.0% displayed typical type-IV N_2 adsorption−desorption isotherms with H_1 hysteresis indicative of mesoporous structure.[22] The attached pore size distribution demonstrated a narrow pore diameter range. Based on the N_2 adsorption−desorption isotherms, the surface area (S_{BET}), pore volume (V_P), and pore diameter (D_P) were calculated. As shown in Table 1, all the Bi_2O_3/TiO_2 samples (including the undoped TiO_2) obtained via the EISA method exhibited much higher S_{BET} than either the P-25 or the Bi_2O_3/TiO_2 (SG) obtained by the traditional sol−gel method, which could mainly be attributed to the presence of mesoporous

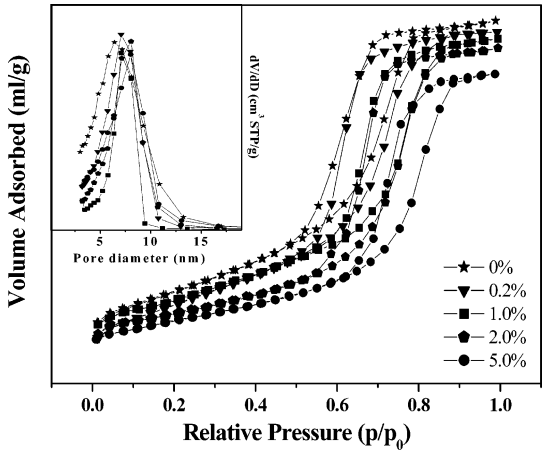

Figure 3. N_2 adsorption−desorption isotherms of Bi_2O_3/TiO_2 calcined at 350 °C. The inset is pore size distribution.

TABLE 1: Structural Parameters and Catalytic Properties of Different Photocatalysts[a]

sample	cal temp (°C)	S_{BET} (m^2/g)	V_p (mL/g)	D_p (nm)	E_g (eV)	degradation (%)
TiO_2	350	174	0.33	6.6	3.2	3
0.20% Bi_2O_3/TiO_2	350	168	0.30	7.0	3.0	26
1.0% Bi_2O_3/TiO_2	350	167	0.29	7.2	2.8	49
2.0% Bi_2O_3/TiO_2	350	158	0.27	7.6	2.8	39
5.0% Bi_2O_3/TiO_2	350	147	0.26	7.8	2.8	21
1.0% Bi_2O_3/TiO_2	300	211	0.34	8.7	2.8	3
1.0% Bi_2O_3/TiO_2	400	105	0.21	8.9	2.8	42
1.0% Bi_2O_3/TiO_2(SG)	350	42	0.19	22	2.8	30
P-25	as-received	45	0.20	20	3.1	3

[a] Reaction conditions: 0.050 g of photocatalyst and 50 mL of 1.0×10^{-4} M *p*-chlorophenol aqueous solution, three 150 W xenon lamps (cutoff at 420 nm by a glass filter) 30 cm away from the reaction solution, reaction temperature 303 K, stirring rate 1000 rpm, and reaction period 6 h.

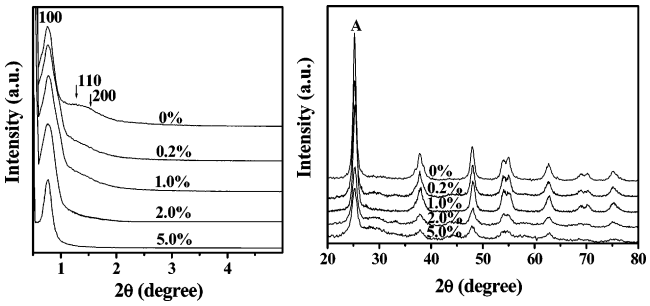

Figure 4. Low-angle XRD (left) and wide-angle XRD (right) of Bi_2O_3/TiO_2 calcined at 350 °C.

structure. For the Bi_2O_3/TiO_2 samples, both S_{BET} and V_P decreased while the D_P increased with enhanced Bi-content, which could be attributed to the blockage of the micropores in the TiO_2 by Bi_2O_3 species.

Figure 4 shows the XRD patterns of Bi_2O_3/TiO_2 samples with different Bi/Ti molar ratios after being calcined at 350 °C. The wide-angle XRD patterns demonstrated that all the samples were present in well-crystallized anatase. No significant shifts of the principal diffraction peaks were observed, indicating that Bi_2O_3 was present in a separate phase adsorbed by TiO_2 rather than incorporated into the TiO_2 lattice, which was in good accordance

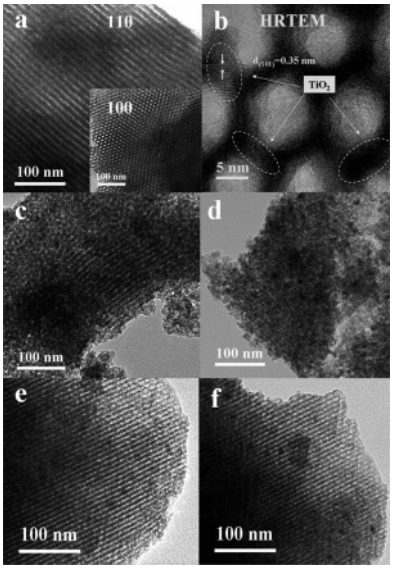

Figure 5. Representative TEM morphologies of 1.0% Bi_2O_3/TiO_2 calcined at 350 °C (a, b), 1.0% Bi_2O_3/TiO_2 calcined at 400 °C (c), and 450 °C (d), 2.0% Bi_2O_3/TiO_2 calcined at 350 °C (e), and 5.0% Bi_2O_3/TiO_2 calcined at 350 °C (f).

with the conclusion from aforementioned XPS spectra. The Bi_2O_3 species were highly distributed in the TiO_2, and thus, no significant diffractional peaks indicative of Bi_2O_3 phase could be observed even at Bi/Ti molar ratio up to 5.0%. However, the crystallization degree of Bi_2O_3/TiO_2 decreased slightly with the increase of Bi/Ti molar ratio, since the presence of Bi_2O_3 disturbed the crystallization process during calcination.[23] The attached low-angle XRD patterns further confirmed that the presence of Bi_2O_3 had very little or even no influence on the ordering degree of the mesoporous structure.

The TEM images (Figure 5a) of the 1.0% Bi_2O_3/TiO_2 calcined at 350 °C displayed highly ordered mesoporous channels with average diameter of ~7.0 nm. The HRTEM image (Figure 5b) showed that the average thickness of the pore walls was ~4.0 nm. Such pore walls were comprised of highly crystallized anatase with the crystalline lattice of 0.35 nm.[24] No significant Bi_2O_3 particles were observed in the pore channels and on the outer surface, implying the extremely high dispersion of the Bi_2O_3 particles, which was consistent with the above conclusion from XRD patterns. The increase of Bi content in the Bi_2O_3/TiO_2 had no considerable effect on the mesoporous structure. But higher Bi content resulted in the appearance of the Bi_2O_3 particles in the pore channels (Figure 5e) and even on the outer surface (Figure 5f). Figure 5c demonstrated that calcination of the 1.0% Bi_2O_3/TiO_2 at 400 °C partially damaged the mesoporous structure. As shown in Figure 5d, the mesoporous structure was completely destroyed after being calcined at 450 °C, which was in good accordance with the results from low-angle XRD patterns.

Optical Properties. As shown in Figure 6a, UV−vis DRS spectra revealed that the undoped TiO_2 displayed no significant absorbance for visible lights due to the large energy gap of TiO_2 (3.2 eV). The Bi_2O_3/TiO_2 calcined at 350 °C showed spectral response in the visible region (λ = 400−600 nm), and the absorbance became stronger with the increase of Bi content from 0.20 to 1.0%. However, further increase of the Bi content had very little influence on the light absorbance. The band energy gap could be calculated by using $(\alpha h\upsilon)^2 = k(h\upsilon - E_g)$, where α is the absorption coefficientm k is the parameter that related to the effective masses associated with the valence and conduc-

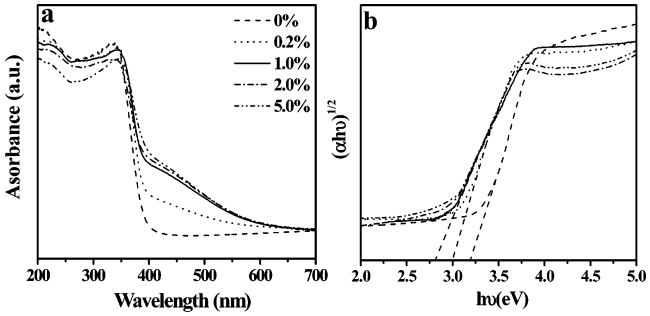

Figure 6. (a) UV−vis DRS spectra and (b) the optical absorption edges (eV) of Bi_2O_3/TiO_2 samples calcined at 350 °C.

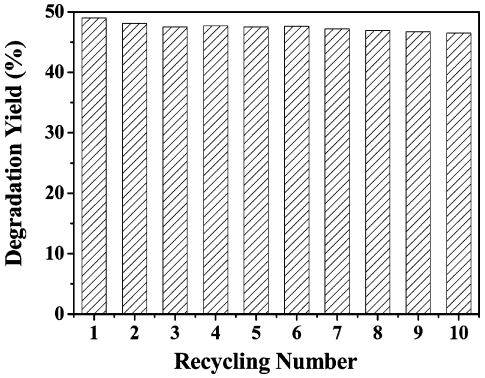

Figure 7. Recycling test of 1.0% Bi_2O_3/TiO_2 calcined at 350 °C. Reaction conditions are given in Table 1.

tion bands, n is $^1/_2$ for a direct transition, $h\upsilon$ is the absorption energy, and E_g is the band gap energy.[25−26] Plotting $(\alpha h\upsilon)^{1/2}$ versus $h\upsilon$ based on the spectral response in Figure 6a gave the extrapolated intercept corresponding to the E_g value (see Figure 6b). As shown in Table 1, the E_g of the Bi_2O_3/TiO_2 calcined at 350 °C decreased with the increase of Bi/Ti ratio from 0.2 to 1.0%. The 1.0% Bi_2O_3/TiO_2 displayed the E_g of 2.8 eV, which was exactly the same as that of the pure Bi_2O_3. The Bi_2O_3/TiO_2(SG) and the 1.0% Bi_2O_3/TiO_2 calcined at either 300 or 400 °C displayed similar E_g values, suggesting that the spectral response in the visible region of the Bi_2O_3/TiO_2 mainly resulted from Bi_2O_3 photosensitization.[6] Briefly, the Bi_2O_3 photosensitizer with narrow energy gap (2.8 eV) could be easily activated by visible lights and induced photoelectrons and holes. In the absence of TiO_2, these electrons and holes might recombine rapidly owing to the narrow energy gap, leading to the quenching of spectral response. In Bi_2O_3/TiO_2, the photoelectrons could easily transfer from the conduct band (CB) of Bi_2O_3 to the neighboring CB of TiO_2. Thus, the recombination between photoelectrons and holes could be effectively inhibited, leading to the strong response in visible area.

Photocatalytic Activity. Table 1 summarizes the activities of various catalysts during photocatalytic degradation of *p*-chlorophenol under irradiation with visible lights (>420 nm). Both the pure TiO_2 prepared by EISA and P-25 available commercially were inactive since these two catalysts could not be activated by visible lights due to a big energy band gap (3.2 eV). Modification of TiO_2 with Bi_2O_3 resulted in abrupt increase of the photocatalytic activity owing to the Bi_2O_3-photosensitization. However, very high Bi content (Bi/Ti molar ratio >2.0%) was harmful for the activity because of the agglomeration of the Bi_2O_3 particles. On one hand, the lower dispersion of Bi_2O_3 reduced its photosentisizing effect, leading to the poor harvesting for visible lights. On the other hand, the big Bi_2O_3 particles resulted in partial blockage of mesoporous channels (see Figure 5f), which may retard the diffusion of reactant molecules.

From Table 1, one could find that the 1.0% Bi_2O_3/TiO_2 obtained via EISA exhibited much higher activity than the 1.0% Bi_2O_3/TiO_2(SG) obtained via the conventional sol−gel method. Since both catalysts exhibited nearly the same crystallization degree of anatase, the higher activity of Bi_2O_3/TiO_2 obtained via EISA could be attributed to its higher S_{BET}, which could enhance the light harvesting and the adsorption for reactant molecules.[8−10,27] Meanwhile, the high S_{BET} was favorable for the dispersion of Bi_2O_3 nanoparticles in the TiO_2, leading to enhanced photosentisizing effect. Furthermore, the ordered mesoporous channels also facilitated the diffusion of reactant molecules.

Considering the effect of calcination temperature on the activity, one could see from Table 1 that the 1.0% Bi_2O_3/TiO_2 calcined at 300 °C exhibited much lower activity than the 1.0% Bi_2O_3/TiO_2 calcined at 350 °C, though it possessed a higher ordering degree of mesoporous structure and higher S_{BET} (Table 1). An important reason was that the 1.0% Bi_2O_3/TiO_2 calcined at 300 °C was present in amorphous state while the 1.0% Bi_2O_3/TiO_2 calcined at 350 °C was present in crystallized anatase. The high crystallization degree of anatase facilitated the rapid transfer of photoelectrons from bulk to the surface, which could effectively inhibit the recombination between photoelectrons and holes, leading to enhanced quantum efficiency.[11−12] However, calcination Bi_2O_3/TiO_2 at high temperature (>400 °C) caused an abrupt decrease in activity, which could be mainly attributed to the damage of mesoporous structure (see Figure 5c and d), taking into account that the crystallization degree of anatase even increased slightly (see Figure 2).

Based on the above results, one could conclude that the 1.0% Bi_2O_3/TiO_2 calcined at 350 °C exhibited the highest activity under visible illumination. Besides the excellent activity, the recycling test (see Figure 7) also demonstrated that this catalyst was quite stable during liquid-phase photocatalysis since no significant decrease in activity was observed even after being used repetitively for 10 times, showing a good potential in practical application.

Conclusions

This work supplied a new approach to prepare Bi_2O_3/TiO_2 with ordered mesoporous structure and highly crystallized anatase based on the EISA method. Such Bi_2O_3/TiO_2 exhibited high photocatalytic activity under visible light irradiation owing to the strong photosensitizing effect of Bi_2O_3 and the unique structural characteristics. On one hand, the Bi_2O_3-photosensitization caused strong spectral response in the visible region. On the other hand, the high surface area and the ordered mesoporous channels enhanced light harvesting, reactant adsorption, and diffusion. Furthermore, the highly crystallized anatase facilitated the transfer of photoelectrons from bulk to surface and thus could inhibit the recombination between photoelectrons and holes, leading to the enhanced quantum efficiency. Other photosensitized TiO_2 visible photocatalysts could also be synthesized by the EISA method, which offers more opportunities for practical application in environmental cleaning.

Acknowledgment. This work was supported by Chinese Committee of Science and Technology (2005CCA01100) and Shanghai Committee of Science and Technology (T0402, 065412070).

References and Notes

(1) Linsebigler, A. L.; Lu, G. Q.; Yates, J. T., Jr. *Chem. Rev.* **1995**, *95*, 735.

(2) De Angelis, F.; Fantacci, S.; Selloni, A.; Nazeeruddin, M. K.; Gratzel, M. *J. Am. Chem. Soc.* **2007**, *129*, 14156.

(3) Clifford, J. N.; Palomares, E.; Nazeeruddin, M. K.; Gratzel, M.; Durrant, J. R. *J. Phys. Chem. C* **2007**, *111*, 6561.

(4) Snaith, H. J.; Gratzel, M. *Adv. Mater.* **2006**, *18*, 1910.

(5) Kay, A.; Cesar, I.; Gratzel, M. *J. Am. Chem. Soc.* **2006**, *128*, 15714.

(6) Bessekhouad, Y.; Robert, D.; Weber, J. V. *Catal. Today* **2005**, *101*, 315.

(7) Kanga, M.; Ko, Y.; Jeon, M.; Lee, S.; Choung, S.; Park, J.; Kim, S.; Choi, S. *J. Photochem. Photobiol., A* **2005**, *173*, 128.

(8) Li, H. X.; Bian, Z. F.; Zhu, J.; Huo, Y. N.; Li, H.; Lu, Y. F. *J. Am. Chem. Soc.* **2007**, *129*, 4538.

(9) Yu, J. C.; Li, G. S.; Wang, X. C.; Hu, X. L.; Leung, C. W.; Zhang, Z. D. *Chem. Commun.* **2006**, 2717.

(10) Yu, J. C.; Wang, X. C.; Fu, X. Z. *Chem. Mater.* **2004**, *16*, 1523.

(11) Hoffmann, M. R.; Martin, S. T.; Chen, W. Y.; Bahnemannt, D. W. *Chem. Rev.* **1995**, *95*, 69.

(12) Fujishima, A.; Rao, T. N.; Tryk, D. A. *J. Photochem. Photobiol., C* **2000**, *1*, 1.

(13) Yang, P. D.; Zhao, D. Y.; Margolese, D. I.; Chmelka, B. F.; Stucky, G. D. *Nature* **1998**, *396*, 152.

(14) Bartl, M. H.; Puls, S. P.; Tang, J.; Lichtenegger, H. C.; Stucky, G. D. *Angew. Chem., Int. Ed.* **2004**, *43*, 3037.

(15) Dong, W. Y.; Sun, Y. J.; Lee, C. W.; Hua, W. M.; Lu, X. C.; Shi, Y. F.; Zhang, S. C.; Chen, J. M.; Zhao, D. Y. *J. Am. Chem. Soc.* **2007**, *129*, 13894.

(16) Antonelli, D. M.; Ying, J. Y. *Angew. Chem., Int. Ed.* **1995**, *34*, 2014.

(17) Crepaldi, E. L.; Soler-Illia, G. J. de A. A.; Grosso, D.; Cagnol, F.; Ribot, F.; Sanchez, C. *J. Am. Chem. Soc.* **2003**, *125*, 9770.

(18) Sakthivel, S.; Kisch, H. *Angew. Chem., Int. Ed.* **2003**, *42*, 4908.

(19) Moulder, J. F.; Stickle, W. F.; Sobol, P. E.; Bomben, K. D.; Chastain, J. *Handbook of X-ray Phototoelectron Spectroscopy*; Perkin-Elmer Corp.: Eden Prairie, MN, 1992; p 191.

(20) Rengaraj, S.; Li, X. Z.; Tanner, P. A.; Pan, Z. F.; Pang, G. K. H. *J. Mol. Catal., A: Chem.* **2006**, *247*, 36.

(21) Alberius, P. C. A.; Frindell, K. L.; Hayward, R. C.; Kramer, E. J.; Stucky, G. D.; Chmelka, B. F. *Chem. Mater.* **2002**, *14*, 3284.

(22) Sing, K. S. W.; Everett, D. H.; Haul, R. A. W.; Moscou, L.; Pierotti, R. A.; Rouquerol, J.; Siemieniewska, T. *Pure Appl. Chem.* **1985**, *57*, 603.

(23) Zhang, J.; Li, M. J.; Feng, Z. C.; Chen, J.; Li, C. *J. Phys. Chem. B* **2006**, *110*, 927.

(24) Yu, J. C.; Wang, X. C.; Wu, L.; Ho, W. K.; Zhang, L. Z.; Zhou, G. T. *Adv. Funct. Mater.* **2004**, *14*, 1178.

(25) Yoon, M.; Seo, M.; Jeong, C.; Jang, J. H.; Jeon, K. S. *Chem. Mater.* **2005**, *17*, 6069.

(26) Peng, X. S.; Meng, G. W.; Zhang, J.; Zhao, L. X.; Wang, X. F.; Wang, Y. W.; Zhang, L. D. *J. Phys. D: Appl. Phys.* **2001**, *34*, 3224.

(27) Rolison, D. R. *Science* **2003**, *299*, 1698.